Evaluation of Strength of Soft Ground Improved by Vacuum Consolidation

T. Shibata[1], S. Nishimura[2], M. Fujii[3] and A. Murakami[4]
[1, 2]*Graduate School of Environmental and Life Science, Okayama University, Okayama, Japan*
[3]*NTC Consultants Co., Ltd., Nagoya, Japan*
[4]*Graduate School of Agriculture, Kyoto University, Kyoto, Japan*
E-mail: tshibata@cc.okayama-u.ac.jp, theg1786@cc.okayama-u.ac.jp, m.fujii@ntc-c.co.jp, akiram@kais.kyoto-u.ac.jp

ABSTRACT: This paper presents the numerical evaluation of the strength and stability of a ground improved via vacuum consolidation combined with a preloading embankment. To assess the stability of soft grounds, the undrained shear strength is definitely required. A numerical analysis is desirable for predicting the strength of the improved ground, and the elasto-plastic FEM for soil-water coupled problems, incorporating the SYS Cam-clay model, is adopted in two dimensions. The compression index of clay and the coefficient of permeability of organic soil, which are the primary factors for evaluating the ground behavior, are identified through an inverse analysis from the measured settlements. As the inverse approach, the particle filter is employed to account for the strong nonlinearity of the ground behavior. A stability analysis of the slip surface method is performed based on the evaluated undrained shear strength to assess the effect of the ground improvement on the construction of earth structures. The results show the validity of the ground improvement using vacuum consolidation with a preloading embankment.

Keywords: Undrained shear strength, Vacuum consolidation, Stability analysis

1. INTRODUCTION

To stabilize soft grounds, some ground improvement techniques are commonly adopted. Many techniques exist, for example, the sand compaction pile method, the vertical drain method, chemical grouting, and so on. Among them, the vertical drain method has been developed within the last thirty years, and prefabricated vertical drains (PVDs) are often employed as the drain material.

The vacuum consolidation method is a kind of vertical drain method. It is a technique for applying vacuum suction to a soft ground to drain the pore water from it. This method is combined with an air-tight sheet and PVDs to promote the consolidation process. A technique for applying vacuum pressure has been introduced, in which vacuum pressure is combined with a special prefabricated vertical drain, called a Cap-drain (CPVD). Besides applying vacuum pressure, embankment loading is used to shorten the consolidation period. The vacuum consolidation method was originally developed by Kjellman (1948) in Sweden. The successful application of vacuum-induced consolidation has continued up to the present. Several studies on the vacuum consolidation method have been reported (Indraratna et al., 2010); numerical and empirical studies in conjunction with PVDs (Chai et al., 2008; Saowapakpiboon et al., 2011) and the smear zone in the immediate vicinity of the PVDs (Indraratna and Redana, 2000) have been investigated.

The method is advantageous in that neither fill material nor heavy machinery is required, and the vacuum pressure method does not put any chemical admixtures into the ground (Chai and Carter, 2011). In addition to these characteristics, isotropic consolidation will induce settlement and inward lateral displacement; thus, there is no possibility of general shear failure in the area of applied vacuum pressure. When a vacuum is applied to a soil mass, it generates negative pore water pressure, and when the total stress is maintained at a constant value, the negative pore pressure causes an increase in the effective stress of the soil. As a result, consolidation can be achieved in the soil at a much faster rate where the PVDs are installed.

To assess the stability of soft grounds, the undrained shear strength is required, which is usually evaluated from field vane tests, unconfined compression tests, undrained triaxial shear strength tests, and the SHANSEP (Stress History and Normalized Soil Engineering Properties) procedure (Ladd and Foote, 1974). The concept of SHANSEP is based on laboratory testing, which attempts to reproduce the conditions of in situ soils. In the SHANSEP technique, UU triaxial compression tests are conducted to provide the shear strength, and clay specimens, normally consolidated and overconsolidated under K_0 conditions, are required. The relationship between the normalized shear strength and the overconsolidated ratio is established from the results of the triaxial compression tests, and the shear strength at the arbitrary depth can be given. The SHANSEP method enables a reliable evaluation of the design parameters; however, the method underestimates the undrained shear strength of the alluvial clay (Tsuchida, 2000).

The undrained shear strength of the ground, improved by vacuum consolidation, has been studied in many published papers. Piezocone and field vane tests are used in their studies (Indraratna et al., 2012; Mersi and Khan, 2012; Yan and Chu, 2005; Saowapakpiboon et al., 2010; Kirstein et al., 2012). Although the mechanism of vacuum consolidation is quite well-understood, difficulties remain in the estimation of the undrained shear strength of the improved ground under various applied loads, such as preloading embankment and vacuum pressure. The numerical estimation can be conveniently used for such difficult problems, including multidimensional loading. In particular, it can be much simpler compared to the SHANSEP procedure, which is based on one-dimensional consolidation and requires high-quality triaxial tests.

In this paper, the undrained shear strength of a ground improved by vacuum consolidation is numerically predicted through a constitutive equation instead of conducting shear tests. The elasto-plastic FEM for soil-water coupled problems is employed as an analytical tool to predict the spatial distribution of the undrained shear strength. The concept of this paper is to present a mixed procedure for the sampled soil tests and the in situ measurement to obtain the undrained shear strength, since the amount of soil tests is often not sufficient. While necessary, the field settlement measurements are conducted in the soft ground engineering. The proposed procedure, based on the inverse analysis to compensate for the shortage of soil tests, is very convenient for engineering purposes.

The ground includes the organic soil layer where the deformation is large; however, it is difficult to decide the soil parameters of the organic soil reasonably. An inverse analysis is a suitable method to obtain the soil parameters using measured data. Since the constitutive parameter of the clay is closely related to that of the organic soil, the compression index of the clay and the coefficient of permeability of the organic soil are identified with an inverse analysis from the measured settlements. As an inverse analysis method, the particle filter (Gordon et al., 1993; Kitagawa,

1996; Higuchi, 2005) is employed here, since the particle filter can easily deal with nonlinear state equations and is robust when employing the Monte Carlo method in conjunction with a numerical simulation, for example, the soil–water coupled finite element analysis with the elasto-plastic model.

The final purpose of this paper is to evaluate the effect of vacuum preloading on the stabilization of the ground for the construction of a dyke at a regulating reservoir. The slip surface method is used to assess the stability. The effect is evaluated by a comparison of the safety factors between the original and the improved states of the ground.

2. GEOMETRY, INSTRUMENTS, AND LABORATORY TESTS

This chapter describes the geometry, the instruments, and the laboratory tests originating from the previous paper (Shibata et al., 2014).

Figure 1 shows a plan view of the regulating reservoir subdivided into 48 blocks under vacuum consolidation combined with the preloading embankment and the observation instruments, such as vacuum pressure gauges, piezometers, hydrostatic settlement cells, and different settlement gauges. A selected portion, indicated by the dark shaded area in Figure 1, is modeled. The target area for this numerical analysis was assumed to be five times as wide as the embankment in order to avoid the influence of the lateral boundaries. The light shaded area, surrounding the reservoir, implies the location where the preloading embankment was constructed. The dotted line along the embankment indicates the center line of the cut-off wall under the ground.

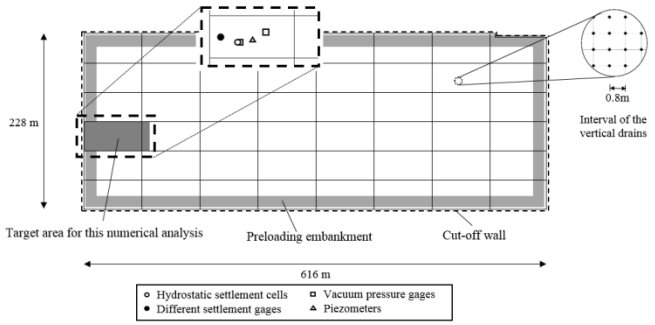

Figure 1 Plan view of regulating reservoir and placement of observation instruments (Shibata et al., 2014)

Figure 2 depicts the problem geometry of the vertical sections of the selected portion along with different stages of the construction sequence. Figure 2(a) shows the initial state; the vacuum pumps connected to the vertical drains started to work in each block, settlement was induced by the vacuum pressure, and then construction of the preloading embankment was started. After the construction of the preloading embankment, seen in Figure 2(b), the vacuum pumping was interrupted and the preloading embankment was removed, as seen in Figure 2(c). Finally, the precast retaining wall was constructed with backfill, as shown in Figure 2(d).

In order to examine the soil profiles and to determine the material properties, a soil investigation was performed by means of rotary drilling and piezocone penetration tests prior to the construction. Piezocone penetration tests give the uniaxial compressive strength and the distribution of excess pore water pressure, which provide the soil profiles for the clay and sand layers. From the results of the rotary drilling, the clay layers were classified into two layers: clay and organic soil.

Unit weight γ, compression index λ, and swelling index κ are determined from laboratory tests. From the tests, the following assumptions that account for the relationship between the swelling index and the compression index of the clay and organic soil can be made as

$$\kappa_o=\lambda_o/6.2 \quad (1)$$

$$\kappa_c=\lambda_c/8.3 \quad (2)$$

where κ_o, λ_o, κ_c, and λ_c indicate the swelling index, the compression index of the organic soil, the swelling index, and the compression index of the clay, respectively.

Additionally, it can be assumed that the compression index of the clay varies directly with that of the organic soil along the critical state line deduced from the results of the laboratory tests as

$$\lambda_o/\lambda_c=4.5135 \quad (3)$$

At the construction site, the settlements and the pore water pressure were measured within the vacuum consolidation process with the preloading, and parameters λ_o and k were determined from the inverse analysis so that the analytical settlement would coincide with the measured settlement. Then, parameters κ_o, κ_c, and λ_c can be determined by Equations (1), (2), and (3), respectively.

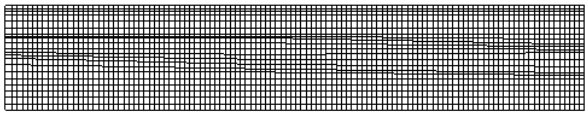

(a) Initial state

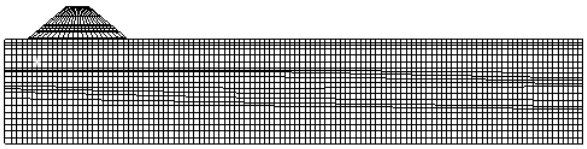

(b) Completion of preloading embankment

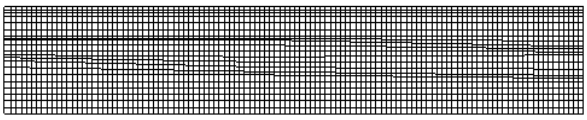

(c) After interruption of vacuum pumping and removal of preloading embankment

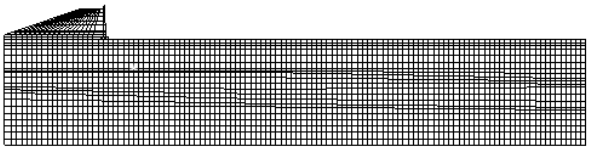

(d) Completion of dyke

Figure 2 Construction process (Shibata et al., 2014)

3. OUTLINE OF INVERSE ANALYSIS

The previous paper presented the identification of the constitutive parameters for the SYS Cam-clay model using the particle filter (Shibata et al., 2014). This chapter presents an outline of the inverse analysis.

The identification of the constitutive parameters for the clay and organic soil of the ground is performed using the actual settlement beneath the preloading embankment for the construction period of vacuum pumping. As the next stage of computation, the numerical prediction is evaluated for the undrained shear strength of the improved ground using the identified parameters.

Figure 3 shows the soil profile of the vertical section to be analyzed based on the soil investigation. The foundation soil consists of alternate layers of clay, organic soil, and sand which are

modeled as elasto-plastic materials. Figure 4 shows the measured settlement used as the observation data of the inverse analysis.

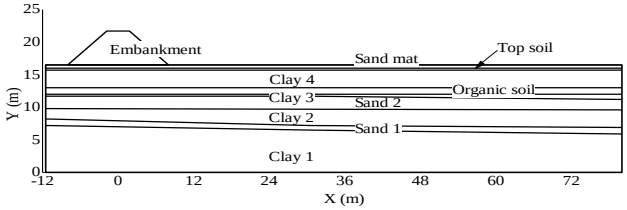

Figure 3 Soil profile (Shibata et al., 2014)

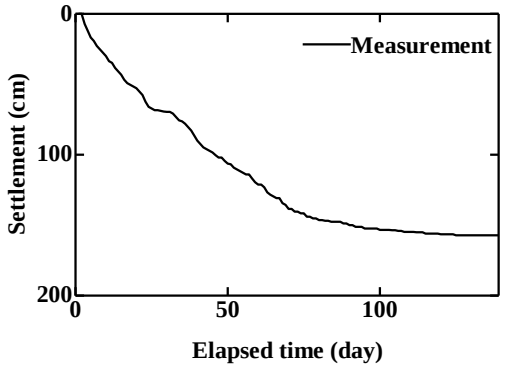

Figure 4 Measured settlement (Shibata et al., 2014)

Figure 5 shows the finite element model, which is generated with 2,554 four-node isoparametric quadrilateral elements with full integration. The associated boundary conditions, in which the width of the element corresponds to the interval of the vertical drains, and the installation of the observation instruments are also depicted in Figure 5. Undrained conditions are assumed on the left side of the ground, because the cut-off wall is constructed along the left side. Permeable boundary conditions are imposed on the bottom and on the right side, and the pore water pressure of the ground surface is set to be 0 throughout the analysis.

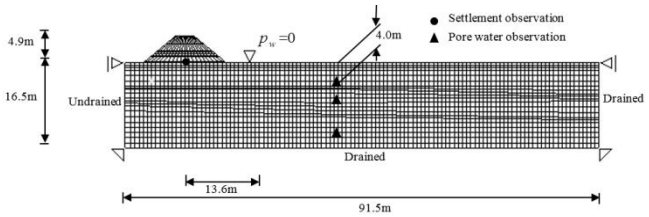

Figure 5 Finite element mesh, boundary conditions, and placement of observation instruments (Shibata et al., 2014)

The bottom boundary is fixed in all directions, while the side boundaries are fixed in only the horizontal direction, such that vertical displacement is allowed. The depth profiles of the initial effective stress and the consolidation yield stress obtained from the consolidation tests, over the entire foundation, are depicted in Figure 6. From the conducted tests, the overconsolidation state is assumed in the shallow layer. Negative pressure of -80 kPa is applied to both left and right sides of the finite element mesh as the suction induced by the vertical drain during vacuum pumping. The time interval of 1 day is used for the analysis. The SYS Cam-clay model (see APPENDIX), proposed by Asaoka et al. (2002), is adopted because the high porosity related to the high water content in the organic soil can be expressed in terms of the high degree of the soil structure, and the numerical computation is performed by means of a soil-water coupled finite deformation analysis incorporating the constitutive model. Figure 7 shows the loading process for the embankment construction and the history of the vacuum pressure, derived from the field observation of the piezometers and the vacuum pressure gauges.

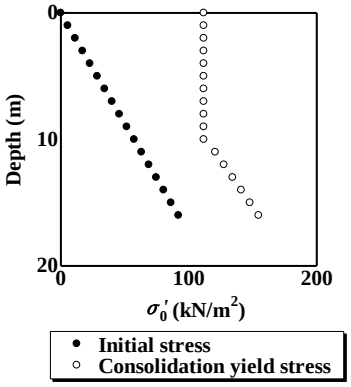

Figure 6 Depth profiles of initial stress and consolidation yield stress

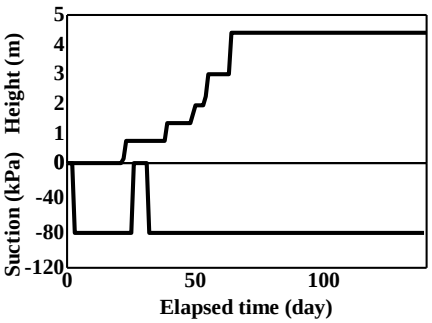

Figure 7 Construction loading process (Shibata et al., 2014)

The values for the soil parameters are shown in Table 1, in which ν is Poisson's ratio, k is the coefficient of permeability, $1/R_0$ is the initial degree of overconsolidation, $1/R_0^*$ is the initial degree of the structure, M is the critical state constant, e_0 is the standard void ratio at p'=98 kPa, p' is the mean effective stress, m is the degradation parameter of the overconsolidated state, and a, b, and c are the degradation of the parameters of the structure, (Kaneda et al., 2009).

Table 1 Soil parameters (Shibata et al., 2014)

	ν	γ (kN/m^3)	k (cm/s)	$1/R_0$
Clay/Silt	0.4	14.5	1.0×10^{-9}	1.429
Sand	0.3	17.7	1.0×10^{-6}	1.429
Organic soil	0.45	11.8	(2.0×10^{-6})	1.429
Topsoil	0.3	14.5	1.0×10^{-8}	1.429
Embankment	0.3	14.5	1.0×10^{-9}	1.429

	$1/R^*_0$	M	e_0	λ
Clay/Silt	2.4	1.2	2.2	(0.740)
Sand	2.4	1.36	0.821	0.07
Organic soil	2.4	1.0	4.921	(3.340)
Topsoil	2.4	1.2	2.2	0.740
Embankment	2.4	1.2	2.2	0.740

	κ	m	a	b, c
Clay/Silt	(0.09)	2.5	0.2	1.0
Sand	0.009	0.01	0.1	1.0
Organic soil	(0.539)	2.5	0.2	1.0
Topsoil	0.09	2.5	0.2	1.0
Embankment	0.09	2.5	0.2	1.0

In Table 1, the values in the parentheses represent the initial values for the identification. The initial values stem from the results of laboratory tests. As mentioned previously, we make assumptions that consider the strong relationship between the compression index and the swelling index, and the compression index of the clay and that of the organic soil are directly proportional to each other deduced from the laboratory tests. Therefore, the compression index of the clay, λ_o, is related to three parameters, namely, the swelling index of the clay, κ_c, the compression index of the clay, λ_c, and the swelling index of the organic soil, κ_o.

The particle filter, based on Sequential Importance Sampling (SIS) (Doucet et al., 2000), is used for the parameter identification, because its sampling scheme has been proven to be advantageous in solving inverse problem for the elasto-plastic deformation of the ground (Shuku et al., 2012; Murakami et al., 2013). 200 sets of particles are generated as uniform random numbers within the range of $0.378 \leqq \lambda_c \leqq 1.115$ and $5.0 \times 10^{-7} \leqq k \leqq 5.0 \times 10^{-6}$ (cm/s). The settlement just beneath the embankment was used as the observation data up to 139 days, at which time the vacuum pump was interrupted and the embankment was removed. The diagonal term for the error covariance matrix, R_{ij}, is assumed as $R_{ij}=(\xi S)^2\delta_{ij}$, where S represents the presumed maximum settlement, ξ is the scalar parameter, and δ_{ij} is Kronecker's delta. Parameter ξ means the coefficient of variation in the maximum settlement; it plays a role in adjusting the information level of the probability density function of the observation noise, namely, the smaller value for ξ corresponds to the more informative probability density function. The values for the scalar parameter are chosen as 0.1, and the system noise is assumed to be zero throughout the analysis. The values for the identified parameters, namely, λ_c of 0.801 and k of6.63×10^{-7} (cm/s), are obtained. κ_c of 0.097, κ_o of 0.581, and λ_o of 3.601 can be determined from the parameter value, namely, λ_o of 0.801.

Figure 8 compares the simulated results using the identified parameters with the measured data, and the numerical results simulate very well the observation data. It is clear that the effectiveness of the PF approach in treating vacuum consolidation problems has been presented through these results.

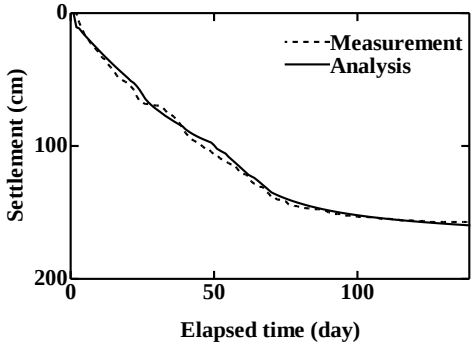

Figure 8 Comparison of settlement beneath embankment between results using identification parameters and corresponding observation data (Shibata et al., 2014)

4. UNDRAINED SHEAR STRENGTH AND EVALUATION OF STABILITY

The evaluation of the undrained shear strength is described after the interruption of the vacuum pumping and the removal of the preloading embankment. The finite element mesh and the boundary conditions are given in Figure 9, while the loading history of the dyke is given in Figure 10. Figure 11 shows an enlarged view of the dyke for which the dark gray shaded area is the precast retaining wall and the brown shaded area is the backfill. The soil parameters in Table 1 are used, where the parameters identified by the inverse analysis are given in lieu of the values in the parentheses. The Young's modulus, Poisson's ratio, and the density of the precast retaining wall are taken to be 2.5×10^{10} (N/m^2), 0.2, and 23.0 (kN/m^3), respectively.

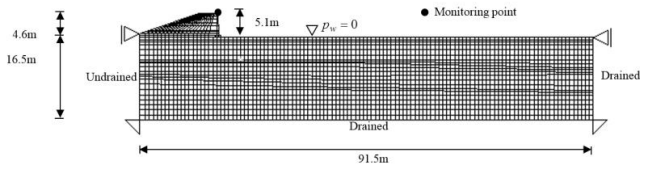

Figure 9 Finite element mesh and boundary conditions (Shibata et al., 2014)

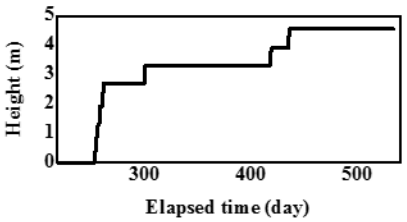

Figure 10 Height of backfill versus time (Shibata et al., 2014)

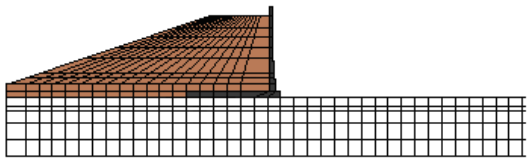

Figure 11 Enlarged view of dyke

Figure 12 illustrates the horizontal displacement of the crown. There are slight differences between the results of the analysis and the measured displacement. Since the horizontal displacement is significantly small, compared with the vertical one, the evaluation of the stability of the ground is not affected by the difference in displacements.

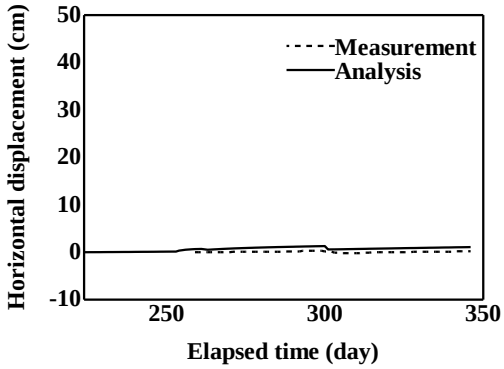

Figure 12 Comparison of precast retaining wall horizontal displacement in crown (Shibata et al., 2014)

4.1 Estimation of undrained shear strength

We briefly describe the undrained shear strength, c_u, for the SYS Cam-clay model. The original Cam-clay model, with the super-subloading yield surfaces, is used in the following calculations. For simplification, however, the effect anisotropy, which is properly considered in the SYS Cam-clay model, is eliminated

herein. The volume change under undrained condition, ε_v, is represented by the SYS Cam-clay model as follows:

$$\varepsilon_v = \frac{\lambda}{1+e_0}\left(\ln\frac{p'}{p'_0} + \ln R^* - \ln R\right) + D\left(\frac{q}{p'}\right) = 0 \quad (4)$$

where $1/R$ is the degree of overconsolidation, $1/R^*$ is the degree of the structure, p'_0 is the initial mean effective stress, and q is the deviator stress. In Eq.(4), ε_v=0 expresses no volume change, because under an undrained condition means an incompressible condition. The critical state at the undrained condition is expressed as

$$\mathrm{M}_s - \frac{q}{p'} = \frac{\lambda-\kappa}{D(1+e_0)} - \frac{q}{p'} = 0 \quad (5)$$

$$\mathrm{M}_s = \mathrm{M}\left(1 - \frac{DU^*}{R^*} + \frac{DU}{R}\right) \quad (6)$$

where U and U^* are positive scalar functions of R and R*, respectively (see APPENDIX).
Substituting p' in Eq. (4) into (5) gives

$$\frac{q}{p'_0} = \frac{R}{R^*}\cdot \mathrm{M}_s \exp\left(-\frac{\lambda-\kappa}{\lambda}\right) \quad (7)$$

Since the undrained shear strength is half the difference of the principal effective stress, we can obtain

$$\frac{c_u}{p'_0} = \frac{R}{R^*}\cdot \frac{\mathrm{M}_s}{2} \exp\left(-\frac{\lambda-\kappa}{\lambda}\right) \quad (8)$$

Figure 13 illustrates the distribution of the undrained shear strength obtained by Eq. (8). The shaded areas indicate the sand layers, where the undrained shear strength is not employed, and the effective internal friction angle is used, since drained conditions exist in the sand layers.

The simulation results at the different stages of the construction sequence are shown in Figures 13 (a)-(d) corresponding to Figures 2 (a)-(d); (a) the initial state, (b) completion of the preloading embankment, (c) after the interruption of the vacuum pumping and the removal of the preloading embankment, and (d) the completion of the dyke. In Figures 13 (b)-(d), it can be seen that the undrained

shear strength of the organic soil increases significantly, and the strength after the ground improvement is more than seven times that in the initial condition in Figure 13 (a). The mean increases of 8% and 23% in the strength of the clay are presented after the ground improvement and the completion of the backfill, respectively.

Figures 14 (a) and (b) show the profiles of the undrained shear strength with depth of the center-line of the preloading embankment and at a distance of 40 m from the center-line of the preloading embankment, respectively. In the figure, four states are compared, where Case (1) is the initial state, Case (2) is the state of the completion of the preloading embankment and subsequent consolidation, Case (3) is the state after interruption of vacuum pumping and the removal of the preloading embankment, and Case (4) is the state of the completion of the precast retaining wall with backfill. In Figures 14 (a) and (b), the undrained shear strength of the organic soil, which exists at a depth of 5 m from the surface, increases significantly.

The original Cam-clay model shows that the critical state line, q=Mp', is the watershed between not only plastic volume compression and plastic volume expansion, but also hardening and softening.Volume compression is always accompanied by hardening, and volume expansion is accompanied by softening. However, the SYS Cam-clay model can express softening with plastic volume compression and hardening with volume expansion. This is because the SYS Cam-clay model gives two critical state lines, q=M$_s$ p' and q=M p', which are the watershed between hardening and softening, and volume compression and volume expansion, respectively (see details in Asaoka et al. 2000). Therefore, this constitutive model can express the peak before the effective stress path reaches the effective failure envelope.

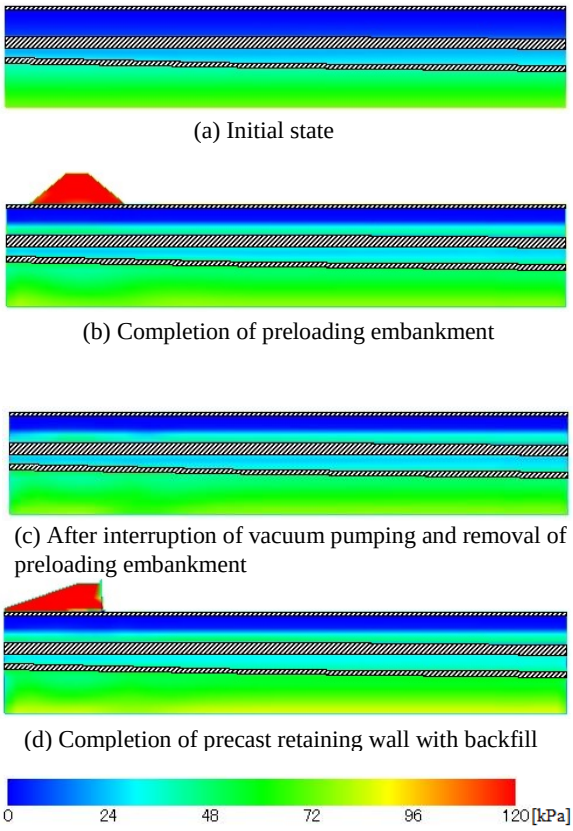

(a) Initial state

(b) Completion of preloading embankment

(c) After interruption of vacuum pumping and removal of preloading embankment

(d) Completion of precast retaining wall with backfill

Figure 13 Distribution of undrained shear strength

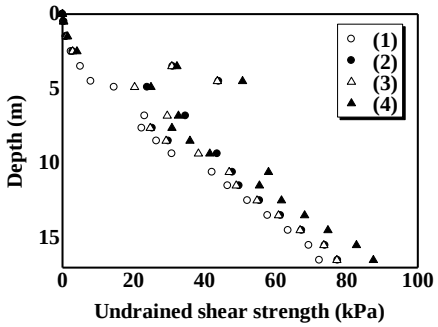

(a) At center-line of preloading

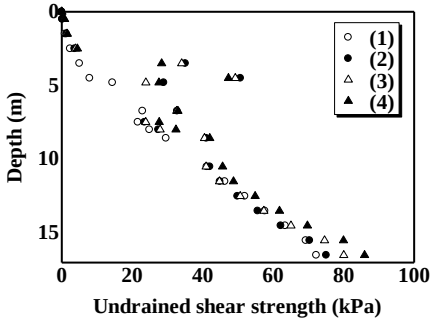

(b) At distance of 40 m from center-line of preloading

Figure 14 Profiles of undrained shear strength with depth

4.2 Stability analysis

To evaluate the effect of the ground improvement for the construction of the dyke surrounding the regulating reservoir, the slip surface method is applied. The following three ground states are analyzed: (a) vacuum consolidation combined with the preloading embankment, (b) only vacuum consolidation, and (c) without ground improvement. The undrained shear strength in Figure 15 is used for the stability analysis.

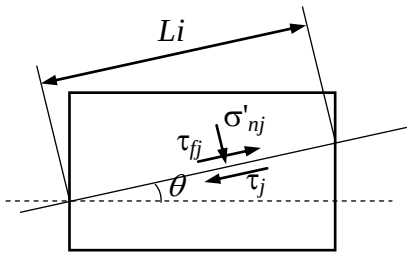

Figure 15 Slip surface across an element

The slip surface method can be performed according to the following steps:

Step 1: Assume the coordinate of the center point and the radius of the circular slip surface.

Step 2: Derive the normal and the shear stresses on the *j*th element, σ'_{nj} and τ_j, along the slip surface from Eqs. (9) and (10), respectively, as shown in Figure 15.

$$\sigma'_{nj} = \frac{\left(\sigma'_{xj} + \sigma'_{yj}\right)}{2} + \frac{\left(\sigma'_{xj} - \sigma'_{yj}\right)}{2}\cos 2\theta_j - \tau_{xyj}\sin 2\theta_j \qquad (9)$$

$$\tau_j = \frac{\left(\sigma'_{xj} - \sigma'_{yj}\right)}{2}\sin 2\theta_j + \tau_{xyj}\cos 2\theta_j \qquad (10)$$

where σ'_{xj} and σ'_{yj} are the vertical and the horizontal stresses on the *j*th element, τ_{xyj} is the shear stress on the *j*th element, and θ_j is the angle between the horizontal plane and the slip surface.

Step 3: Derive the shear strength on the *j*th element, τ_{fj}, from the Mohr-Coulomb law of Eq. (11).

$$\tau_{fj} = c_j + \sigma'_j \tan\phi_j \qquad (11)$$

where c_j is the cohesion on the *j*th element and ϕ_j is the friction angle on the *j*th element.

Step 4: The factor of safety, F_s, is given by

$$F_s = \Sigma\tau_j L_j / \Sigma\tau_{fj} L_j \qquad (12)$$

in which L_j, is the length of the slip surface within the *j*th elements.

Steps 1 to 4 are iterated for the several slip surfaces derived from the different centroids and the radii, and then, the minimum value for F_s is determined as the factor of safety. In Step 3, the cohesion is the undrained shear strength of the clay and the organic soil; it is set to be zero for the sand layer. The friction angles of the clay and the organic soil take the values of zero, and a friction angle of 33.67 degrees is assumed for the sand.

Figure 16 shows the results of the stability analysis for the three ground states along with the critical slip surfaces. There are slight differences in the centroids and the radii among the different ground states; however, all slip surfaces pass across the top soil, the sand mat, and the clay layer. Table 2 lists the factors of safety corresponding to the assumed ground states. It can be seen that the stability is increased due to the vacuum consolidation, because the factor of safety for the ground after the improvement is 0.20 larger than that of the case without ground improvement. This is an increase in the factor of safety caused by the vacuum consolidation method; therefore, it is confirmed that the advantages of the method are the shortened consolidation period and the strength increment of the soft soil. When the vacuum consolidation is combined with a preloading embankment, a significant increase in the factor of safety is shown.

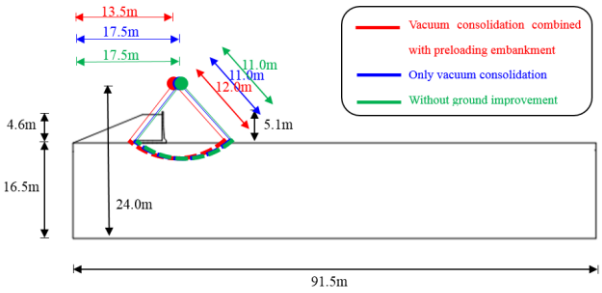

Figure 16 Slip surface on improved ground

Table 2 Factor of safety

Ground state	Factor of safety
Vacuum consolidation combined with preloading embankment	1.104
Only vacuum consolidation	0.763
Without ground improvement	0.566

Table 3 indicates the vertical displacement during the construction of the dyke. According to the table, the effectiveness of the vacuum consolidation combined with preloading embankment is shown, since the settlement value of the case is significantly reduced compared with the case without ground improvement. The preloading embankment leads to the settlement, thereby compacting the soil around the embankment. In Table 3, the vertical displacement of the crown is small when the vacuum consolidation method is combined with the preloading embankment; however, the vertical displacement is large when only the vacuum consolidation is applied. In Table 2, the factor of safety for the case with only the vacuum consolidation is slightly larger than that for the case without ground improvement. The clay near the ground surface has a large region of elastic behavior and a high yield point, and the vertical displacement in the case with only vacuum consolidation is large. However, the applied stress exceeds the elastic region in the case with vacuum consolidation combined with preloading embankment, and plastic deformation takes place; therefore, the small vertical displacement is obtained.

Table 3 Vertical displacement at the top of crown

Ground state	Vertical displacement (cm)
Vacuum consolidation combined with preloading embankment	16.1
Only vacuum consolidation	31.5
Without ground improvement	39.0

5. CONCLUSIONS

This paper has presented an evaluation of the effect of vacuum preloading for the stability of the ground for the construction of a dyke for a regulating reservoir. In order to assess the stability, the undrained shear strength of the ground was numerically predicted in conjunction with an elasto-plastic FEM for soil-water coupled problems, incorporating the SYS Cam-clay model.

The compression index of the clay and the coefficient of permeability for the organic soil were identified with the inverse analysis based on the actual settlement. As the inverse approach, the particle filter was adopted to overcome the strong nonlinearity of the ground response to the loading.

The undrained strength was determined based on the parameters identified by the inverse analysis. The strength of the organic soil significantly increased with the ground improvement, and the strength value was more than four times that in the initial condition. To assess the effect of the improvement, a slip surface analysis was carried out using the evaluated undrained shear strength. Since the factor of safety of the improved ground was 0.20 larger than that of the unimproved ground, it has been revealed that the vacuum consolidation is effective. There is a significant increase in the factor of safety when vacuum consolidation is combined with a preloading embankment.

Additionally, the vertical displacement during the construction of the dyke was compared through the analysis. When vacuum consolidation with the preloading embankment was applied, the vertical displacement was drastically reduced.

Considering the results of the stability and settlement analyses, it has been clarified that the ground improvement, combining vacuum consolidation and the preloading embankment, is a very effective way to stabilize soft grounds.

6. ACKNOWLEDGEMENTS

The valuable suggestions and comments by Professor Feng Zhang of the Nagoya Institute of Technology and Dr. Kazuhiro Kaneda of Takenaka Corporation, and help with the numerical analysis by Ms. Yu Masutani of the Graduate School of Kyoto University are gratefully acknowledged. This work was supported by Grant-in-Aid for Challenging Exploratory Research Grant Number 23656297 from the Japan Society for the Promotion of Science (JSPS) KAKENHI.

7. APPENDIX

7.1 The SYS Cam-clay model

The modified Cam-clay yield function, which can describe the anisotropy behavior (Noda et al., 2005), is expressed as

$$\begin{aligned} &f\left(\tilde{p}',\tilde{\eta}^{*}\right)+\int_0^t J\,\mathrm{tr}D\,d\,\tau \\ &=\mathrm{MD}\ln\frac{\tilde{p}'}{\tilde{p}_0'}+\mathrm{MD}\ln\frac{\mathrm{M}^2+\tilde{\eta}^{*2}}{\mathrm{M}^2}+\int_0^t J\,\mathrm{tr}D^{P}\,d\,\tau=0 \end{aligned} \tag{13}$$

where f is the yield function, $\tilde{p}'$ is the projected stress parameter on the normal surface, $\tilde{\eta}^{*}$ is the anisotropy stress ratio, t is the current time, J is the Jacobian determinant of deformation gradient tensor $\boldsymbol{F}$, $\boldsymbol{D}$ is the stretching tensor, M is the critical state parameter, D is the dilatancy parameter, $\tilde{p}_0'$ is the mean effective stress, and $\boldsymbol{D}^{\mathrm{p}}$ is the plastic part of the stretching tensor.

The superloading surface is assumed to lie above the normal surface. The similarity ratio of the normal surface to the superloading surface in terms of stress, denoted by R^{*}, lies between zero and one ($0<R^{*}\le 1$). The subloading surface is again assumed to be geometrically similar to the superloading surface. The similarity ratio of the subloading surface to the superloading surface in terms of stress, denoted by R, takes the value between zero and one ($0<R\le 1$). Based on Eq. (13), the current stress state is on the subloading surface as follows:

$$\begin{aligned} &f\left(p',\eta^{*}\right)+\mathrm{MD}\ln R^{*}-\mathrm{MD}\ln R+\int_0^t J\,\mathrm{tr}D\,d\,\tau \\ &=\mathrm{MD}\ln\frac{p'}{\tilde{p}_0'}+\mathrm{MD}\ln\frac{\mathrm{M}^2+\eta^{*2}}{\mathrm{M}^2}+\mathrm{MD}\ln R^{*}-\mathrm{MD}\ln R \\ &+\int_0^t J\,\mathrm{tr}D^{P}\,d\,\tau=0 \end{aligned} \tag{14}$$

where $R^{*}=\tilde{p}'/\bar{p}'=\tilde{q}/\bar{q}$, $R=p'/\bar{p}'=q/\bar{q}$, and $\bar{q}$, $\bar{p}'$ and $\tilde{q}$, $\tilde{p}'$ are the projected stress parameters on the superloading and the normal-yield surfaces and correspond to current stress parameters q and p'. The anisotropy stress ratio parameter is defined by $\eta^{*}=\sqrt{3\hat{\eta}\cdot\hat{\eta}/2}$, where $\hat{\eta}=\eta-\beta$, $\eta=S/p'$, $S=T'+p'I$, $\boldsymbol{I}$ is the unit tensor, and $\boldsymbol{\beta}$ is the rotational hardening tensor. Evolution rules for R^{*}, R, and $\boldsymbol{\beta}$ are given as follows:

$$\dot{R}^{*}=JU^{*}\left\|D_S^{p}\right\|,\ U^{*}=\frac{a}{\mathrm{D}}R^{*b}\left(1-R^{*}\right)^{c} \tag{15}$$

$$\dot{R}=JU\left\|D^{p}\right\|,\ U=-\frac{m}{\mathrm{D}}\ln R \tag{16}$$

$$\mathring{\beta}=J\frac{b_r}{\mathrm{D}}\sqrt{\frac{2}{3}}\left\|D_S^{p}\right\|\left\|\hat{\eta}\right\|\left(m_b\frac{\hat{\eta}}{\left\|\hat{\eta}\right\|}-\beta\right) \tag{17}$$

where m is the degradation parameter of the overconsolidated state, a, b, and c are the degradation of the parameters of the structure, m_b is the limit of rotation, and b_r is the evolution parameter of anisotropy.

Plastic multiplier, λ, is obtained by the associated flow rule, namely,

$$\lambda=\frac{\frac{\partial f}{\partial T'}\cdot\mathring{T}'}{J\frac{\mathrm{MD}}{p'\left(\mathrm{M}^2+\eta^{*2}\right)}\left(\mathrm{M}_{\mathrm{s}}^2-\eta^2\right)} \tag{18}$$

where

$$\begin{aligned} \mathrm{M}_{\mathrm{s}}^2&=\mathrm{M}_{\mathrm{a}}^2+b_r\frac{4\mathrm{M}\eta^{*2}}{\mathrm{M}^2+\eta^{*2}}\left(m_b\eta^{*}-\sqrt{\frac{3}{2}}\hat{\eta}\cdot\beta\right)-\sqrt{6}\mathrm{MD}\frac{U^{*}}{R^{*}}\eta^{*} \\ &+\mathrm{MD}\frac{U}{R}\sqrt{6\eta^{*2}+\frac{1}{3}\left(\mathrm{M}_{\mathrm{a}}^2-\eta^2\right)^2} \end{aligned} \tag{19}$$

$$\mathrm{M}_{\mathrm{a}}^2=\mathrm{M}^2+\xi^2,\ \xi=\sqrt{\frac{3}{2}\beta\cdot\beta}=\sqrt{\frac{3}{2}}\left\|\beta\right\|. \tag{20}$$

This study adopts the original Cam-clay model instead of the modified Cam-clay model, and the yield surfaces can be written as follows:

$$\begin{aligned} &f\left(p',\eta^{*}\right)+\mathrm{MD}\ln R^{*}-\mathrm{MD}\ln R+\int_0^t J\,\mathrm{tr}D\,d\,\tau \\ &=\mathrm{MD}\ln\frac{p'}{p_0'}+\mathrm{D}\frac{q}{p'}+\mathrm{MD}\ln R^{*}-\mathrm{MD}\ln R \\ &+\int_0^t J\,\mathrm{tr}D^{P}\,d\,\tau=0 \end{aligned} \tag{21}$$

The plastic multiplier is expressed as follows:

$$\lambda = \frac{\frac{\partial f}{\partial T'} \cdot T'}{J \frac{\mathrm{D}}{p'^2} \left(\mathrm{M}_s p' - q \right)} \tag{22}$$

8. REFERENCES

Asaoka, A., Nakano, M., and Noda, T. (2000). "Superloading yield surface concept for highly structured soil behavior." Soils and Foundations, 40 (2), pp 99-110.

Asaoka, A., Noda, T., Yamada, T., Kaneda, K., and Nakano, M. (2002). "An elasto-plastic description of two distinct volume change mechanisms of soils." Soils and Foundations, 42 (5), pp 47-57.

Chai, J.C., Miura, N., and Bergado, D.T. (2008). "Preloading clayey deposit by vacuum pressure with Cap-drain: Analyses versus performance." Geotextiles and Geomembranes, 26 (3), pp 220-230.

Chai, J.C., and Carter, J.P. (2011). "Deformation analysis in soft ground improvement." Geotechnical, Geological, and Earthquake Engineering, 18, pp 109-171.

Doucet, A., Godsill, S., and Andrieu, C. (2000). "On sequential Monte Carlo sampling methods for Bayesian filtering." Statistics and Computing, 10, pp 197-208.

Gordon, N.J., Salmond, D.J., and Smith, A. F. M. (1993). "Novel approach to nonlinear/non-Gaussian Bayesian state estimation." IEE Proceedings-F, 140 (2), pp 107-113.

Higuchi, T. (2005). "Particle filter." The Journal of the Institute of Electronics, Information and Communication Engineers, 88 (12), pp 989-994 (in Japanese).

Indraratna, B., and Redana, I. W. (2000). "Numerical modeling of vertical drains with smear and well resistance installed in soft clay." Canadian Geotechnical Journal, 37, pp 132-145.

Indraratna, B., Geng, X., and Rujikiatkamjorn, C. (2010). "Review of methods of analysis for the use of vacuum preloading and vertical drains for soft clay improvement." Geomechanics and Geoengineering: An International Journal, 5 (4), pp 223-236.

Indraratna, B., Rujikiatkamjorn, C., Balasubramaniam, A. S., and McIntosh, G. (2012). "Soft ground improvement via vertical drains and vacuum assisted preloading." Geotextiles and Geomembranes, 30, pp 16-23.

Kaneda, K., Watabe, Y., Yamazaki, H., Shinsha, H., and Shiina, T. (2009). "Mechanism of vacuum consolidation using soil water coupled analysis and application." Japanese Geotechnical Journal, 4 (3), pp 245-258 (in Japanese).

Kitagawa, G. (1996). "Monte Carlo filter and smoother for non-Gaussian nonlinear state space models." Journal of Computational and Graphical Statistics, 5 (1), pp 1-25.

Kjellman, W. (1948). "Accelerating consolidation of fine grain soils by means of cardboard wicks." Proceedings of the 2nd ICSMFE, 2, pp 302-305.

Kirstein, J., and Wittorf, N. (2012). "Rigid inclusions in combination with fast wick drain consolidation as soil improvement method in very soft and fat northern German clay." ISSMGE - TC 211 International Symposium on Ground Improvement IS-GI Brussels.

Ladd, C. C., and Foote, R. (1974). "A new design procedure for stability of soft clays." Journal of the Geotechnical Division, 100, GT7, pp 763-786.

Mesri, M., and Khan, A. Q. (2012). "Ground improvement using vacuum loading together with vertical drains." Journal of Geotechnical and Geoenvironmental Engineering, 138, pp 680-689.

Murakami, A., Shuku, T., Nishimura, S., Fujisawa, K., and Nakamura, K. (2013). "Data assimilation using the particle filter for identifying the elasto-plastic material properties of geomaterials." International Journal for Numerical and Analytical Methods in Geomechanics, 37 (11), pp 1642-1669.

Noda, T., Asaoka, A.,Nakano, M., Yamada, E., and Tashiro, M. (2005). "Progressive consolidation settlement of naturally deposited clayey soil under embankment loading." Soils and Foundations, 45 (5), pp 39-51.

Saowapakpiboon, J., Bergado, D. T., Youwai, S., Chai, J. C., Wanthong, P., and Voottipruex, P. (2010). "Measured and predicted performance of prefabricated vertical drains (PVDs) with and without vacuum preloading." Geotextiles and Geomembranes, 28, pp 1-11.

Saowapakpiboon, J., Bergado, D.T., Voottipruex, P., Lam, L.G., and Nakakuma, K. (2011). "PVD improvement combined with surcharge and vacuum preloading including simulations." Geotextiles and Geomembranes, 29 (1), pp 74-82.

Shibata, T., Murakami, A., and Fujii, M. (2014). "Prediction of embankment behavior of regulating reservoir with foundation improved by vacuum consolidation method." Soils and Foundations, in press.

Shuku, T., Murakami, A., Nishimura, S., Fujisawa, K., and Nakamura, K. (2012). "Parameter identification for Cam-clay model in partial loading model tests using the particle filter." Soils and Foundations, 52 (2), pp 279-298.

Tsuchida, T. (2000). "Evaluation of undrained shear strength of soft clay with consideration of sample quality." Soils and Foundations, 40 (3), pp 39-42.

Yan, S. -W., and Chu, J. (2005). "Soil improvement for a storage yard using the combined vacuum and fill preloading method." Canadian Geotechnical Journal, 42, pp 1094-1104.